

Thermally driven self-healing efficient flexible perovskite solar cells

Yangjie Lan^{a,1}, Yang Wang^{a,*1}, Yue Lai^{b,1}, Zheren Cai^a, Mingquan Tao^a, Yuduan Wang^a, Mingzhu Li^{a,c}, Xia Dong^{b,c,*}, Yanlin Song^{a,c,*}

^a Key Laboratory of Green Printing, Institute of Chemistry Chinese Academy of Sciences, Beijing 100190, PR China

^b Beijing National Laboratory for Molecular Sciences, CAS Key Laboratory of Engineer Plastics, Institute of Chemistry Chinese Academy of Sciences, Beijing 100190, PR China

^c University of Chinese Academy of Sciences, Beijing 100049, PR China



ARTICLE INFO

Keywords:
Thermally driven
Self-healing
Flexible
Perovskite
Solar cells

ABSTRACT

The brittleness of perovskite (PVK) film restrains the development and application of the flexible perovskite solar cells (FPSCs). We utilize the polyurethane elastomers with disulfide bonds (PUDS) as a self-healing polymer to construct self-healing FPSCs and strengthen the self-healed perovskite film by the phase-locked state. The PUDS efficiently enhances the flexibility and self-healing properties of FPSCs. The champion efficiencies of MAPbI₃ on rigid and flexible substrates with PUDS are 20.30% and 17.19%, respectively. Importantly, the efficiency of cracked FPSC after thermal self-healing (80 °C) has been recovered from 12% (Broken: 2.06%) of the initial efficiency (17.19%) to 88% (Recovery: 15.12%). Besides, the efficiency of FPSC with PUDS maintains 95% of the initial value after 3000 h stored in glove box. This strategy provides an effective approach for developing flexible electronics.

1. Introduction

Perovskite solar cells (PSCs) have rapidly emerged as a central player for high-performance photovoltaics [1–5]. Especially, flexible perovskite solar cells (FPSCs) have attracted extensive attention due to their mechanical flexibility, lightness and low-costs [6–8]. At present, the nature property of perovskite fragility restrains the flexibility and application of the FPSCs [9,10]. The flexible performance of perovskite film is relating to the minimum bending radius and the number of the bending cycles [11–13]. To increase the flexibility of the FPSCs, there are many reported strategies, such as interface engineering, constructing micro-nano structures [14,15] and adding flexible long-chain polymers [16]. These methods have been utilized to improve the crystalline quality and the flexibility to avoid the bending damage of FPSCs caused by the stress concentration [17,18]. Since the ignored key point that the multiple bending cycles cause the rapid decrease and irreversible recovery of PCE, the self-healing methods of devices have been studied. For instance, organic molecules or polymer scaffolds strengthened and repaired crystals to realize the self-healing [19]; intrinsic repairing property of the perovskite to realize the recovered efficiency of the

FPSCs in a dark environment [20,21] and liquid metal repaired the scratched electrode realizing the recovery of efficiency [22]. However, the self-healing perovskite, as an effective approach to achieve the recovery of device, has rarely been reported.

Herein, we utilize the polyurethane elastomers with disulfide bonds (PUDS) to fabricate the self-healing FPSCs. PUDS is consisted of hard phase and soft phase, resulting in the good tensile properties and bending resistance. Disulfide bonds in the hard phase have a lower stimulus response temperature ($T_S = 60^\circ\text{C}$). The broken disulfide bonds can easily form free radicals as the temperatures beyond T_S [23,24]. The sulfur in the free radical state can forms disulfide bonds with the nearest free radical when the temperature is cooled to realize self-healing, the schematic diagram is shown in Fig. 1a. Furthermore, due to the coordination between carbonyl (C=O) with Pb²⁺ [25,26], the grain size and quality of perovskite films have been obviously improved. Meanwhile, the efficiencies of PSCs with PUDS reach 20.30% (rigid substrate) and 17.19% (flexible substrate) with less hysteresis, retaining 95% of the initial PCE after 3000 h stored in glove box. Besides, the FPSC also obtains good flexibility, achieving 84% of the initial value (17.19%) even after 4000 bending cycles at a radius of 3 mm. Significantly, the disulfide

* Corresponding authors at: Beijing National Laboratory for Molecular Sciences, CAS Key Laboratory of Engineer Plastics, Institute of Chemistry Chinese Academy of Sciences, Beijing 100190, PR China.

E-mail addresses: wangyang@iccas.ac.cn (Y. Wang), xiadong@iccas.ac.cn (X. Dong), [ylysong@iccas.ac.cn](mailto:ylsong@iccas.ac.cn) (Y. Song).

¹ These authors contributed to this work equally.

bonds in PUDS can assist the thermally driven self-healing of cracked perovskite film caused by the bending destruction (bending radius: 2 mm) when the annealing temperature exceeds the stimulus response temperature ($T_s = 60^\circ\text{C}$). The efficiency of the cracked FPSC recovers

from 12% (Broken: 2.06%) to 88% (Recovery: 15.12%) of the initial efficiency (17.19%).

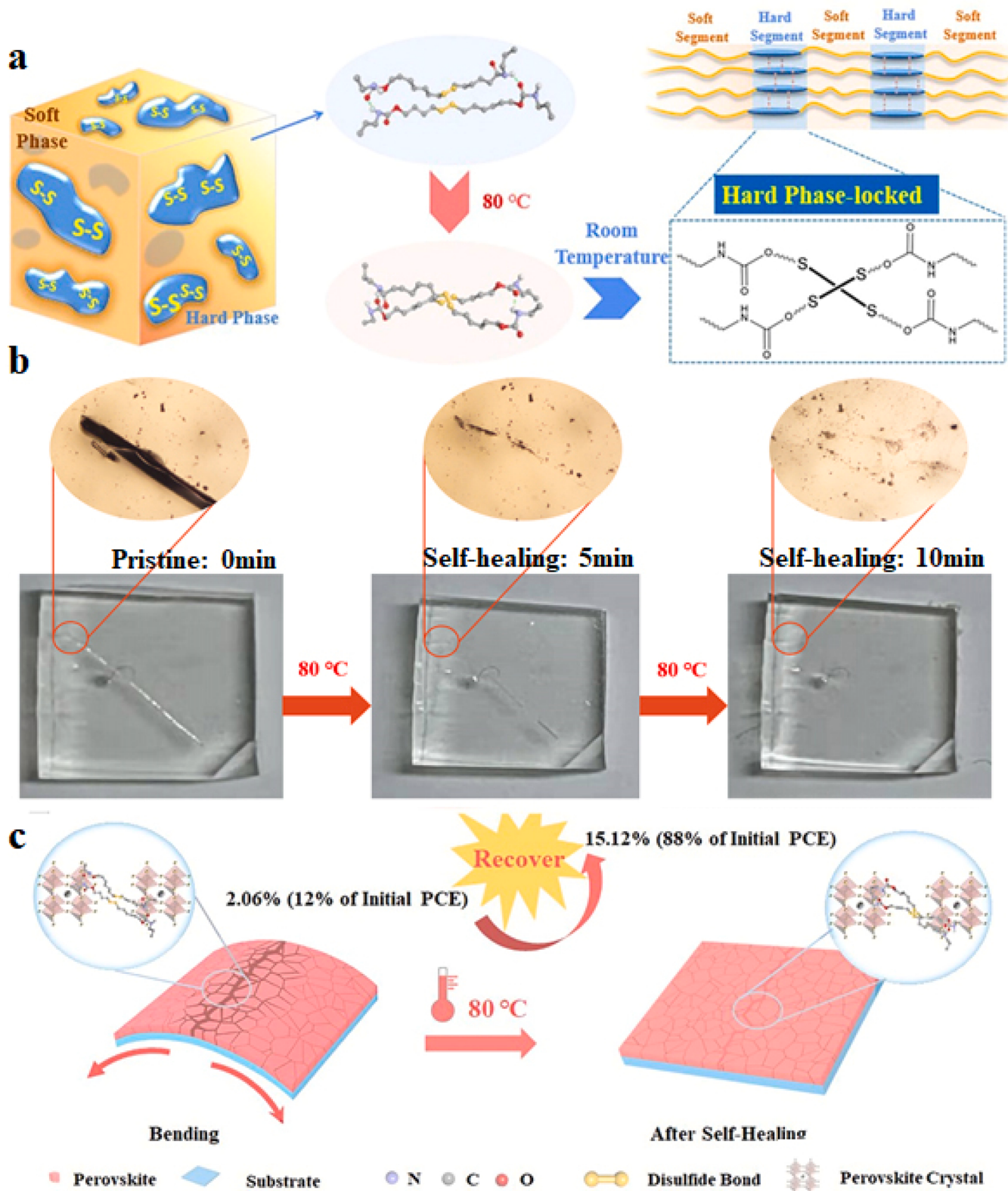


Fig. 1. (a) Schematic diagram of the self-healing process of PUDS. (b) Optical microscope images of the manual crack self-healing process under continuous heat treatment (80°C) over time. (c) The schematic diagram of self-healing process of the perovskite film with PUDS.

2. Experiment section

2.1. Materials

Indium Tin Oxide (ITO) coated polyethylenenaphthalate (PEN) (sheet resistance is less than 10 ohm/sq, transmittance is more than 85%) purchased from Liaoning Youxuan Co.,Ltd. Methylamine iodide ($\text{CH}_3\text{NH}_3\text{I}$, 99.0%), lead (II) iodide (PbI_2 , 99.0%), [6,6]-Phenyl-C₆₁-butyric acid methyl ester (PC₆₁BM), poly (ethylene imine) (PEI) are purchased from Xi'an Baolaite. N, N-Dimethylformamide (DMF, AR), dimethyl sulfoxide (DMSO, AR), chlorobenzene (CB, anhydrous, 99.8%), $\text{Ni}(\text{NO}_3)_2 \cdot 6 \text{H}_2\text{O}$, NaOH and isopropanol are purchased from Sigma-Aldrich. Acetone (AR) and ethanol (AR) are purchased from Beijing Chemical Works. Ag (99.99%) is purchased from China New Metal Materials Technology Co., Ltd. NiO_x nanocrystals (NCs) are synthesized according to procedures as the following. First, 0.1 mol Ni (NO_3)₂ · 6 H₂O were dissolved in 100 mL of deionized (DI) water to obtain a green colloidal. Then, NaOH solution (10 mol L⁻¹) was slowly added into the solution while magnetic stirring. When the pH value of the colloid just reached 10, the colloid was washed with DI water three times by centrifugal washing. The colloid precipitation was vacuum dried at 80 °C overnight and obtained green powder, then calcined at 270 °C for 2 h to obtain a dark-black powder.

2.2. Solution preparation

0.461 g PbI_2 and 0.159 g MAI (molar ratio of 1:1) are dissolved in 1 mL mixed solvent of anhydrous DMF and anhydrous DMSO (volume ratio 4:1). PUDS is dissolved in the mixed solution (DMF: DMSO = 4:1) (0 mg/mL, 0.05 mg/mL, 0.1 mg/mL, 0.2 mg/mL, 0.5 mg/mL, 1 mg/mL, 2 mg/mL, 5 mg/mL). The NiO_x NCs solution were prepared by dispersing the NiO_x NCs in DI water with a concentration of 30 mg/mL, stirred the solution for 5 min, then filtered by using the 0.22 μm polyethersulfone filter.

2.3. Device fabrication

The flexible substrate (PEN/ITO) is washed by DI water, acetone, ethanol, isopropanol in ultrasonic 20 min and dry with nitrogen gas. Flexible substrate (PEN/ITO) is adhered on the glass (1.5 cm × 1.5 cm) by PDMS (polydimethylsiloxane). Then the substrates are treated with O₂-plasma for 15 min. The prepared NiO_x NCs solution is deposited onto the substrate by spin-coating at 3000 rpm for 30 s, transferring the substrate to the hot plate at 120 °C for 30 min. After that, substrates are transferred into the glove box. The $\text{CH}_3\text{NH}_3\text{PbI}_3$ precursor solution is deposited onto the substrates by spin-coating at 1000 rpm for 5 s with the acceleration of 1000 r/s, then 5000 rpm for 40 s with the acceleration of 1000 rpm. The 120 μL chlorobenzene is quickly dropped onto the substrates at the last 25 s of the spin coating. Transferred the substrate to the hot plate at 100 °C for 30 min, the color of the substrate gradually changed from transparent to light brown, dark brown, and black. After annealing, PC₆₁BM and PEI is spin-coating on these substrates at 3000 rpm for 40 s and 5000 rpm for 60 s, respectively. Finally, Ag electrode (100 nm) is deposited on PEI layer by thermal evaporation. The PSCs with the structure of glass or PEN/ITO/NiO_x/perovskite/PC₆₁BM/PEI/Ag.

2.4. Characterization

Morphology of perovskite films are measured by the field-emission scanning electron microscope (SEM, JEOL, JSM-7500 F, Japan). The XRD patterns are measured by the D8 FOCUS powder diffractometer (Bruker). Absorbance spectra are measured by the UV-vis spectroscopy photometer (Perkin Elmer Lambda 750). The J-V curves are measured under AM 1.5 G solar irradiation at 100 mW/cm² (Enli Tech, Class AAA solar simulator). The external quantum efficiency (EQE) is measured

illumination with monochromatic (Enli Tech, Class AAA solar simulator, QE-mini) at the wavelength range of 300–850 nm. The bending radius test is to continuously bend the flexible PSCs on a plastic rod with a defined radius. The Young's modulus has been measured toward layer by layer using Nano Test Vantage (Micro Materials). Simulations were performed using the commercial finite element software COMSOL 5.4.

3. Results and discussion

The PSC consists of Glass or Polyethylene naphthalate (PEN)/indium tin oxid (ITO)/NiO_x/Perovskite/[6,6]-phenyl-C₆₁-butyric acid methyl ester (PC₆₁BM)/polyether imide (PEI)/Ag, as shown in Fig. S1. The PUDS as self-healing polymer is consisted of soft phase and hard phase in Fig. 1a. The manual crack of millimeter-scaled width is gradually healed over 10 min under heat treatment at 80 °C, as shown in Fig. 1b. The disulfide bonds in the PUDS molecule have low molecular mobility when temperature below the stimulus response temperature (T_s , 60 °C) [23]. While, it occurs the recombination of disulfide bonds when T (80 °C) > T_s , realizing the self-healing of PUDS through dynamic reaction process. After the annealing temperature cooling to the room temperature, the disulfide bond maintains the stable state by phase-locking. Therefore, we utilize this particular property to construct the self-healing mechanism of FPSCs to repair the FPSC cracks, as shown in Fig. 1c.

The effect of PUDS concentration on the perovskite grain size is summarized in Fig. S2. The carbonyl in the PUDS have the strong interaction with Pb²⁺, retarding the crystallization rate of the perovskite and promoting the crystallization process of the crystal, increasing the size of the crystal. After optimization, the grain size of perovskite film with 1 mg/mL PUDS is much larger than the pristine (up to 1.8-fold), as shown in Fig. 2a and b. In addition, the vertical growth of perovskite crystals of the perovskite with PUDS has a significant improvement (Fig. S3). In Fig. S4, the root-mean-square (RMS) surface roughness of the perovskite films without and with PUDS are 7.3 nm and 11.4 nm, respectively. It indicates that the PUDS can efficiently reduce the surface roughness of perovskite film, which is beneficial to increase ohmic contact between perovskite and electron transfer layer and further improve device performances. Moreover, X-ray diffraction (XRD) is utilized to characterize the crystal quality of the perovskite film. In Fig. 2c, the main diffraction peak positions appear at 14.2°, 28.3° and 32.1°, which are corresponding to the planes of the tetragonal perovskite structure of MAPbI₃ [27–29]. Compared with the pristine, the diffraction peak intensity of perovskite film with PUDS is obviously enhanced. Furthermore, the half-width of perovskite film with PUDS (0.284°) is narrower than the pristine (0.318°), indicating the crystallinity of the perovskite film with PUDS has been enhanced. As show in Fig. 2d, there is an obvious shift of the peak positions of Pb 4 f_{7/2} and 4 f_{5/2} to higher binding energy, which is correlating to the existence of the chemical interaction between Pb²⁺ and PUDS. In addition, the peak of O 1 s has an obvious low bonding energy shift due to the coordination of the carbonyl group in the PUDS with the Pb²⁺ (Fig. S5). While, the peak of S 2p of the PUDS in perovskite has no obvious shift, indicating that the disulfide bonds are not coordinated with perovskite (Fig. S6).

Ultraviolet-visible (UV-vis) spectrophotometry and steady-state photoluminescence (PL) spectra are used to measure the quality of the perovskite films, as shown in Fig. 2e. The perovskite film with PUDS shows stronger absorption and higher PL intensity than the pristine. The PL intensity of the perovskite film with PUDS is about 2.1 times comparing with the pristine. Overall, the PUDS can efficiently reduce the surface defects of the perovskite film and improve the crystalline quality [30–32]. The time-resolved photoluminescence (TRPL) decay is employed to quantify the photoluminescence lifetime of perovskite films. Fitting the TRPL decay curves with the biexponential decay function as: ($y = A_1 \exp(-t/\tau_1) + A_2 \exp(-t/\tau_2) + y_0$) [33,34], where A_1 and A_2 represent the relative amplitude, τ_1 and τ_2 represent the carrier lifetime for fast and slow recombination, respectively. The fast decay τ_1

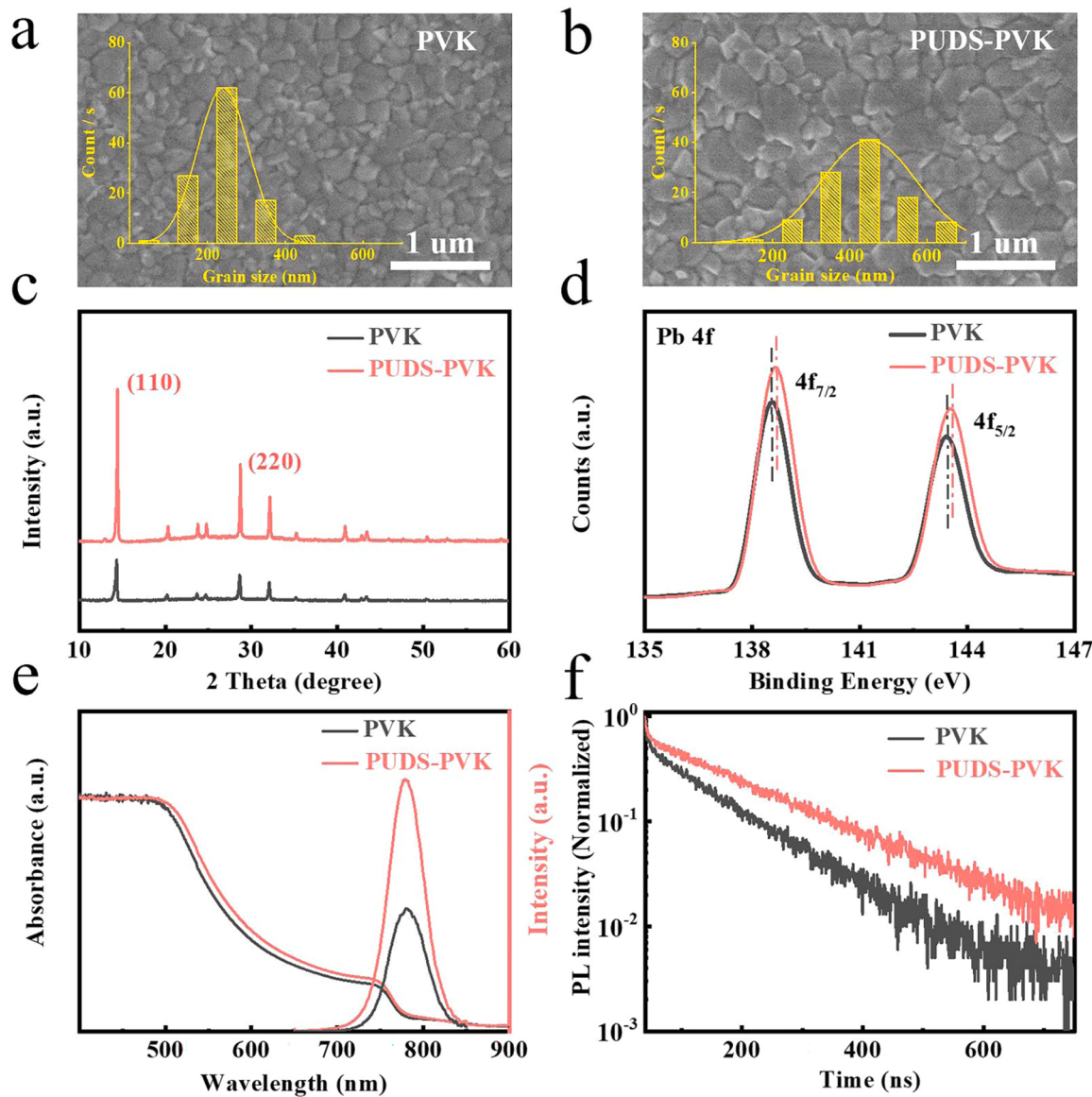


Fig. 2. Analysis of the perovskite films with PUDS and without PUDS. (a and b) SEM images of the perovskite films without and with PUDS, respectively. (Inset: the histogram of crystal size distribution) (c) XRD patterns. (d) X-ray photoelectron spectroscopy (XPS) spectra of Pb 4 f in the perovskite films. (e) UV-vis absorption and steady-state photoluminescence spectra of perovskite films without and with PUDS on glass substrates. (f) TRPL decay spectra of perovskite films without and with PUDS on glass substrates.

is relating to the surface recombination. The slow decay τ_2 is correlating to the radiative recombination and the carriers lifetime before the carriers recombination, also reflecting the carriers diffusion length. In Fig. 2f, the pristine perovskite film shows faster decay than the PUDS-perovskite film. The perovskite film with PUDS exhibits fast and slow phase lifetimes of $\tau_1 = 9.54$ ns (fraction $A_1 = 0.02$) and $\tau_2 = 240.74$ ns (fraction $A_2 = 0.98$), respectively. While, the pristine exhibits $\tau_1 = 59.09$ ns (fraction $A_1 = 0.26$) and $\tau_2 = 107.93$ ns (fraction $A_2 = 0.74$), respectively. The photoluminescence lifetime of perovskite films with different PUDS concentrations are summarized in Table S1. From the results of the TRPL, the perovskite film with PUDS obtains high crystal quality and low defects, accelerating interfacial charge separation and transportation. Moreover, Fig. S7 reveals the energy level arrangements of various functional layers in the PSCs. The conduction band (VB) and valence band (CB) can be calculated by ultraviolet photoelectron spectroscopy (UPS), as shown in Fig. S8 and Fig. S9. The VB and CB of perovskite film with PUDS shift from -6.0 eV and -4.4 eV to -5.5 eV and -3.9 eV, which can boost carriers transport

and enhance the open circuit voltage (V_{oc}) of devices.

Based on the above excellent performances, the PSCs with the PUDS have been fabricated. A series of rigid PSCs with the different PUDS contents based on the plane device configuration consisting of the indium tin-oxide (ITO) substrate/ NiO_x /Perovskite/PC₆₁BM/PEI/Ag (Fig. S10 and Table S2. Fig. 3a exhibits the current density (J)-voltage (V) characteristic of the PSCs without and with PUDS under the standard AM 1.5 G solar illumination with a light intensity of 100 mW/cm^2 from 1.2 V to -0.1 V at a scan ratio of 0.02 V/s . The corresponding photovoltaic parameters are summarized in Table S3. The rigid substrate without PUDS shows a power conversion efficiency (PCE) of 17.20% , with a V_{oc} of 1.08 V , short circuit current (J_{sc}) of 21.14 mA/cm^2 and fill factor (FF) of 75.36% . While, the PCE of the PSC with PUDS on a rigid substrate increases to 20.30% , with a V_{oc} of 1.14 V , a J_{sc} of 28.88 mA/cm^2 and FF of 78.21% with less hysteresis index (HI). The hysteresis index is defined as: $\text{HI} = \frac{(\text{PCE}_{\text{Forward}} - \text{PCE}_{\text{Reverse}})}{\text{PCE}_{\text{Reverse}}} \times 100\%$ [35–37], where PCE Reverse and PCE Forward represent PCE obtained from J-V measurement in reverse scan and forward scan, respectively. The HI of PSC with

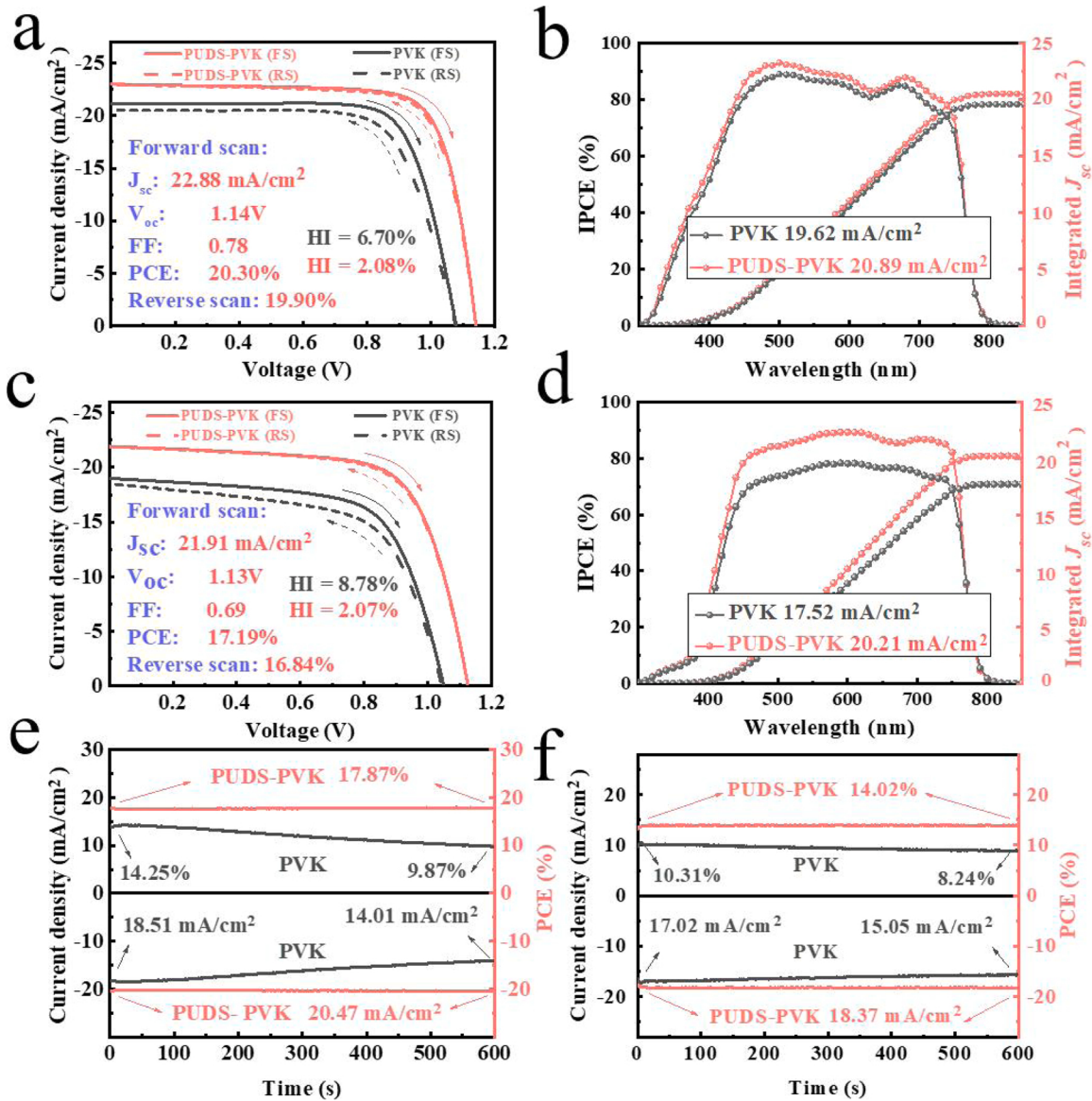


Fig. 3. *J-V* curves of the PSCs with rigid (a) and flexible (c) substrates. The EQE curves of PSCs with rigid (b) and flexible (d) substrates. (e) Stabilized PCE and photocurrent of the rigid PSCs without and with PUDS measured at a bias of V_{max} under 1 solar illumination intensity. (f) Stabilized PCE and photocurrent of the rigid PSCs without and with PUDS measured at a bias of V_{max} under 1 solar illumination intensity.

PUDS is 2.08%, which is lower than the pristine (6.21%). In addition, J_{sc} is in good agreement with the integrated value from the incident photon-to-current conversion efficiency (IPCE) spectra, as shown in Fig. 3b. We also fabricate the FPSC with PUDS in Fig. S11 and Table S4. After optimization, the champion PUDS-FPSC with less HI reaches a PCE of 17.19%, a V_{oc} of 1.13 V, a J_{sc} of 21.91 mA/cm² and FF of 69.47%, which are much higher than that of the pristine. The integrated J_{sc} values of the FPSCs from IPCE is in good agreement with the J_{sc} from the *J-V* measurement, as shown in Fig. 3d. The corresponding photovoltaic parameters of the FPSCs are summarized in Table S5. Fig. S12 shows the statistics of PSCs performances for rigid and flexible PSCs without and with PUDS based on 25 devices. The serious *J-V* hysteresis caused by ion migration tend to occur at defects between grain boundaries in perovskite [38–40]. Fig. 3e and f show the stabilized current density and the PCE of PSCs and FPSCs without and with PUDS, respectively. These results suggest that the PSCs and FPSCs with PUDS can significantly enhance the stability of the devices.

The V_{oc} dependence upon light intensity is applied to represent the charge-carrier recombination characteristics, as shown in Fig. 4a. The

ideal slope is $1kT/q$, where k is the Boltzmann constant, T is the absolute temperature in Kelvin, and q is the elementary charge. Comparing with the pristine (1.25), the PSC with PUDS has a lower slope (1.12). This indicates that trap-assisted recombination for PSC with PUDS is effectively suppressed. The relation between J_{sc} and illumination intensity is described by the formula of $J_{sc}\propto I^{\alpha}$, as shown in Fig. S13. The slope of PSCs (0.962) with PUDS is bigger than the pristine (0.924), indicating that all free carriers are swept out and collected at electrodes before recombination. Furthermore, the space-charge-limited current (SCLC) is further applied to evaluate the effect of PUDS on the defect-states of the perovskite films. In Fig. 4b, the device shows linear ohmic-type response at low bias voltage. Once the voltage surpasses the kink point, named the trap-filled limit voltage V_{TFL} , the current displays significant enhancement due to the trap states completely filled by the injected carriers. The trap density (N_t) can be determined through V_{TFL} by the equation [41–44]: $V_{TFL} = eN_t L^2/2\epsilon\epsilon_0$, where e , N_t , ϵ , ϵ_0 and L represent the elementary charge, trap density, the relative dielectric constant of the perovskite, the vacuum permittivity and the thickness of the perovskite films, respectively. The relative dielectric constant is 46.9 for the

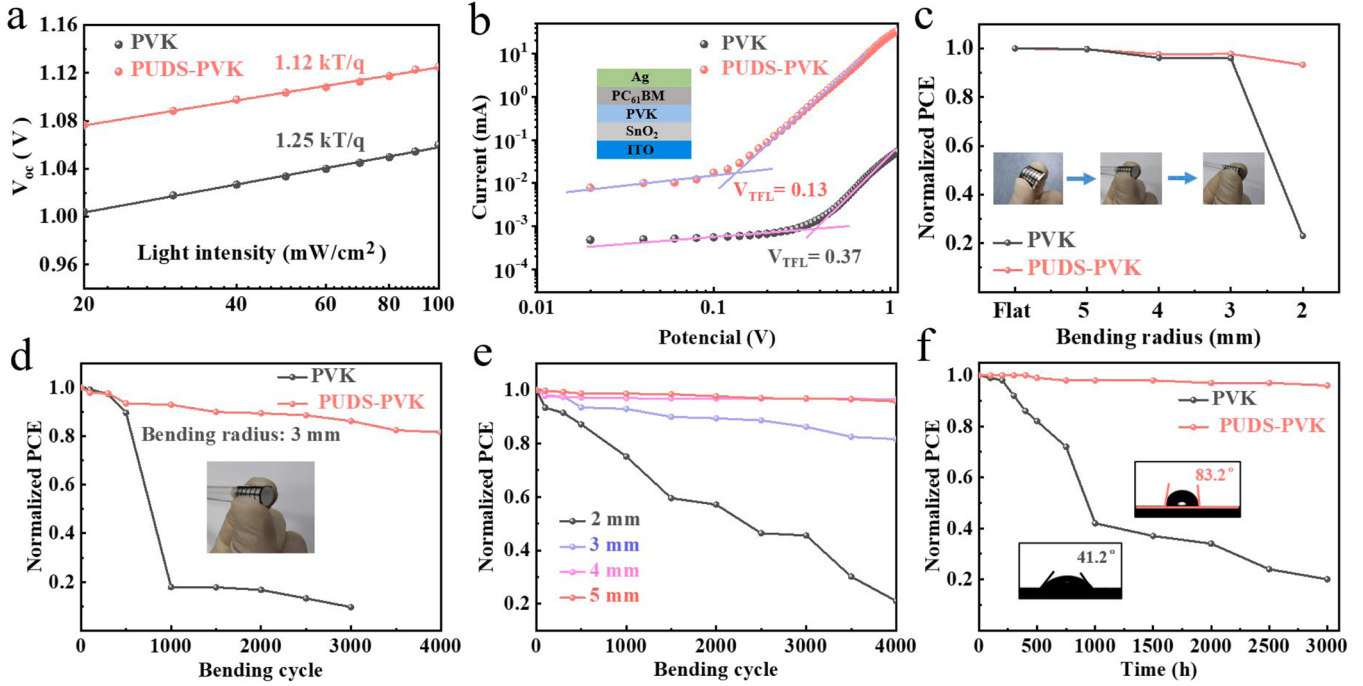


Fig. 4. (a) V_{oc} versus incident light intensity for PSCs without and with PUDS. (b) Dark current-voltage curves for devices without and with PUDS. (c) Normalized PCE v.s. bending radius of FPSCs without and with PUDS after 100 bending cycles. (d) Normalized PCE v.s. bending cycles of FPSCs without and with PUDS under 3 mm radius. (e) Normalized PCE v.s. bending cycles of FPSCs with PUDS under different radii. (f) Long-term stability of devices stored in a glove box.

MAPbI_3 [44] and the thickness of the perovskite film is about 420 nm. Perovskite film with PUDS has a remarkably low trap density $N_t = 1.70 \times 10^{15} \text{ cm}^{-3}$ comparing with the pristine (N_t (pristine) = $4.32 \times 10^{15} \text{ cm}^{-3}$), which is responsible for improving the photoelectric performance of device. Due to the high quality of the perovskite film, the dark current density of the FPSC with PUDS is significantly reduced, as shown in Fig. S14. The small dark current leakage also demonstrates that the perovskite film with PUDS has fewer defects. Moreover, the electrochemical impedance spectroscopy (EIS) is carried out to characterize the charge recombination resistance of FPSCs. The Nyquist plots of the FPSCs with PUDS and the pristine are shown in Fig. S15. Recombination resistance (R_{rec}) and the contact resistance (R_{co}) are attributed to electron-hole recombination and electron extraction, respectively. The R_{rec} of the FPSCs with PUDS significantly has been improved from 4202Ω to 7109Ω , whereas the R_{co} has been reduced from 234Ω to 133Ω . The higher R_{rec} and the lower R_{co} of the FPSCs with PUDS, attributing to passivate the trap states and reduce the carrier recombination [45].

To validate the impact of mechanical bending on the flexibility properties of FPSCs, the normalized PCE of FPSCs is measured after bending 100 cycles under different radii of curvature (from 5 mm to 2 mm), as shown in Fig. 4c. The FPSCs without and with PUDS can maintain the excellent performance after bending when the bending radius is 3 mm. When the bending radius reaches 2 mm, the efficiency of FPSCs without PUDS decrease sharply, while the FPSCs with PUDS can still maintain 94% of the initial efficiency. Thus, we test the influence of bending cycles on the PCE of the FPSCs at a radius of curvature (3 mm), as shown in Fig. 4d. The FPSC with PUDS maintains 84% of the initial PCE after 4000 bending cycles. In contrast, the pristine sharply decreases to 14% of the initial PCE. In Fig. 4e, the PCE of the FPSCs with PUDS is stable even for small radius of curvature, ascribing the ability of the PUDS elastomer to enhance the mechanical flexibility and durability of perovskite film. Due to the stress concentration during the bending process, the PCE quickly decreases under the 4000 bending cycles at the radius of 2 mm. The contact angle (for a water droplet) of the perovskite film without and with PUDS has been measured, as shown in inset of

Fig. 4f. The contact angle of the perovskite film with PUDS (83.2°) is greater than the pristine (41.2°), indicating that the additive of PUDS contributes to the hydrophobicity of the perovskite film so that the FPSCs retain 95% of the initial PCE over 3000 h, as shown in Fig. 4f.

Furthermore, the young's modulus of the PSCs is measured by layer-by-layer, the data are summarized in Table S6 and Table S7. Based on the corresponding mechanical parameters, the finite-element method is carried to simulate the stress distribution perovskite. Fig. 5a and b show the finite element simulation of the stress distribution of a perovskite film on PEN substrate with the hole transport layer of NiO_x . The flexuous perovskite film with PUDS shows a uniform stress distribution, while the pristine shows the state of concentrated stress. The FPSC with PUDS achieves a uniform stress distribution under the bending, which significantly enhances the flexibility and bending life of the FPSCs. In Fig. S16, the FPSC with PUDS obtains the uniform stress distribution, which is better than the pristine. Irreversible damage occurs for FPSCs after many bending cycles, it brings a significant limitation to practical applications of devices. Therefore, we verify the self-healing mechanism of FPSCs by thermal heating. We utilize the atomic force microscope (AFM) to characterize the self-healing process, as shown in Fig. 5c. The perovskite film has obvious cracks after many bending cycles under the radius of 2 mm, where the cracks break along the grain boundaries. Interestingly, there are no obvious cracks in the perovskite film after the self-healing process of thermal annealing (80°C 10 min). This property of the self-healing is benefited from the stimuli-responsiveness of the disulfide bonds when the temperature beyond the exchange reaction temperature, which is also higher than the T_g . As the temperature back to the room temperature, the dynamic bonds transform to the phase-locked state strengthening the self-healed perovskite film. As show in Fig. S17, the Micro-Raman spectra characteristic peaks of disulfide bonds after self-healing is not change compared with the characteristic peaks before bending. The schematic diagram of the self-healing process of the cracks is shown in Fig. 5d. As shown in Fig. 5e, we measure the $J-V$ curves of FPSCs under the states of initial, cracked, and self-healing. The fill factor of the FPSCs decreased rapidly, indicating that the devices are damaged. The ions generated as the perovskite crystal is destroyed in the

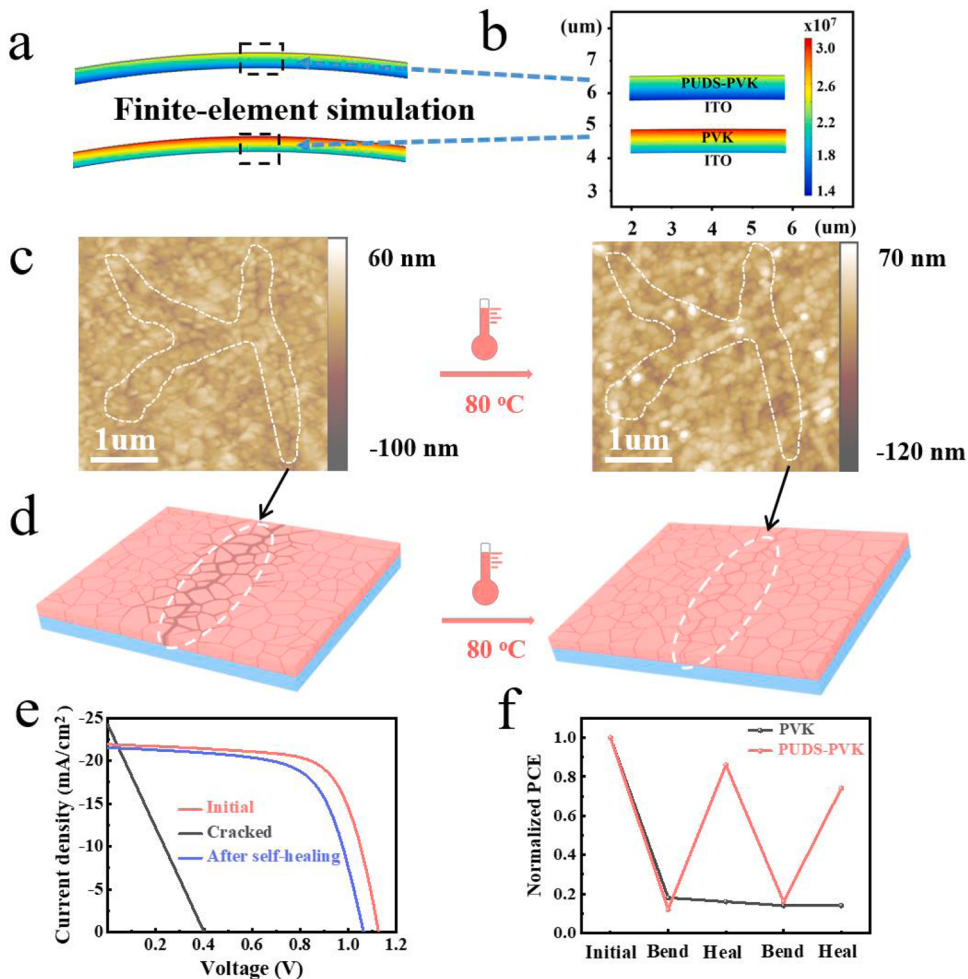


Fig. 5. (a and b) Finite-element simulation of perovskite films without and with PUDS. (c) AFM images of cracks in the perovskite film before (left) and after self-healing (right). (d) Illumination of the cracked perovskite film (left) and the perovskite film after self-heating (right). (e) The J-V curves of FPSCs under the states of initial, cracked, self-healing. (f) Self-healing cycle measurement of FPSCs.

cracked device. The ions participate in the transport of carriers, causing an increase in the number of carriers, so that the J_{sc} of the damaged device is higher than the normal device. After thermal annealing under 80 °C for 10 min, the PCE of the FPSCs with PUDS recovered from 12% (cracked: 2.06%) to 88% (self-healing: 15.12%) of the initial PCE value (17.19%). After the multiple bending-heal, the FPSC with PUDS maintains the 80% (self-healing: 13.71%) of its initial PCE (PCE: 17.01%), while the pristine stays the low PCE due to the cracked perovskite film. To date, the thermal annealing temperature of self-healing PSC is one of the lower thermal annealing temperature comparing with the reported literatures [46,47]. The details of the device structure, annealing temperature, PCE and normalized recovery efficiency are summarized in Table S8. Besides, we further characterize the self-healing cycle of FPSC with PUDS, which also exhibits excellent the self-healing property for FPSC as shown in Fig. 5f.

4. Conclusion

In summary, we introduce the PUDS into the perovskite film to achieve the self-healing of FPSCs and simultaneously improve the efficiency. The PUDS passivates surface defects via the combination between carbonyl (C=O) and Pb²⁺, realizing the grain boundary regulation and defects management. Importantly, PUDS with the disulfide bonds are activated and exchanged as the temperature beyond the corresponding temperature of stimulus, achieving the self-healing flexible perovskite solar cell after cracking. The champion efficiencies

of 17.19% and 20.30% on flexible and rigid substrates are obtained, respectively. Accordingly, it also achieves 88% of the initial power conversion efficiency (17.19%) after the self-healing by thermal annealing at 80 °C. This approach demonstrates a simple way to fabricate highly efficient and self-healing PSCs, which provides an effective strategy to prolong the lifetime and increase the competitiveness of perovskite photovoltaic.

CRediT authorship contribution statement

Yangjie Lan: Writing - Original draft , Writing - Review & Editing, Data curation, Conceptualization, Methodology. **Yang Wang:** Writing - Review & Editing, Conceptualization, Methodology, Validation. **Yue Lai:** Data curation, Conceptualization, Validation. **Zheren Cai:** Software, Validation, Investigation. **Mingquan Tao:** Software, Validation, Investigation. **Yuduan Wang:** Validation, Investigation. **Mingzhu Li:** Formal analysis, Investigation. **Xia Dong:** Writing -Review & Editing, Conceptualization, Methodology, Validation, Supervision. **Yanlin Song:** Writing - Review & Editing, Conceptualization, Methodology, Validation, Supervision.

Declaration of Competing Interest

The authors declare that they have no known competing financial interests or personal relationships that could have appeared to influence the work reported in this paper.

Data availability

Data will be made available on request.

Acknowledgment

Lan, Y.; Wang, Y. and Lai, Y. contributed equally to this work. This work was supported by the National Natural Science Foundation of China (Grant Nos. 52003273, 22073107, 51573192 and 51961145102), Youth Innovation Promotion Association CAS (No. 2022034), K.C. Wong Education Foundation, National Key R&D Program of China (Grant No. 2018YFA0208501), Beijing National Laboratory for Molecular Sciences (BNLMS- CXXM-202005).

Appendix A. Supporting information

Supplementary data associated with this article can be found in the online version at doi:10.1016/j.nanoen.2022.107523.

References

- [1] X. Li, D. Bi, C. Yi, J.-D. Décoppet, J. Luo, S.M. Zakeeruddin, A. Hagfeldt, M. Grätzel, *Science* 353 (2016) 58–62.
- [2] W.S. Yang, B.-W. Park, E.H. Jung, N.J. Jeon, Y.C. Kim, D.U. Lee, S.S. Shin, J. Seo, E. K. Kim, J.H. Noh, S.I. Seok, *Science* 356 (2017) 1376–1379.
- [3] Y. Wang, Z. Zhang, M. Tao, Y. Lan, M. Li, Y. Tian, Y. Song, *Nanoscale* 12 (2020) 18563.
- [4] Y. Wang, Y. Lan, Q. Song, F. Vogelbacher, T. Xu, Y. Zhan, M. Li, W.E.I. Sha, Y. Song, *Adv. Mater.* 33 (2021), 2008091.
- [5] Y.-H. Lin, N. Sakai, P. Da, J. Wu, H.C. Sansom, A.J. Ramadan, S. Mahesh, J. Liu, R. D.J. Oliver, J. Lim, L. Aspitarte, K. Sharma, P.K. Madhu, A.B. Morales-Vilches, P. K. Nayak, S. Bai, F. Gao, C.R.M. Grovenor, M.B. Johnston, J.G. Labram, J. R. Durrant, J.M. Ball, B. Wenger, B. Stannowski, H.J. Snaith, *Science* 369 (2020) 96–102.
- [6] X. Yin, P. Chen, M. Que, Y. Xing, W. Que, C. Niu, J. Shao, *ACS Nano* 10 (2016), 363036.
- [7] E. Cho, Y.Y. Kim, D.S. Ham, J.H. Lee, J.-S. Park, J. Seo, S.-J. Lee, *Nano Energy* 82 (2021), 105737.
- [8] Y. Hu, T. Niu, Y. Liu, Y. Zhou, Y. Xia, C. Ran, Z. Wu, L. Song, P. Müller-Buschbaum, Y. Chen, W. Huang, *ACS Energy Lett.* 6 (2021) 2917–2943.
- [9] H.S. Jung, G.S. Han, N.-G. Park, M.J. Ko, *Joule* 3 (2019) 1850–1880.
- [10] X. Zhang, F. Zabihi, H. Xiong, M. Eslamian, C. Hou, M. Zhu, H. Wang, Q. Zhang, *Chem. Eng. J.* 394 (2020), 124887.
- [11] Y. Lan, Y. Wang, Y. Song, *Flex. Print. Electron.* 5 (2020), 014001.
- [12] Z. Li, Z. Wang, C. Jia, Z. Wan, C. Zhi, C. Li, M. Zhang, C. Zhang, Z. Li, *Nano Energy* 94 (2022), 106919.
- [13] M. Li, W.W. Zuo, A.G. Ricciardulli, Y.G. Yang, Y.H. Liu, Q. Wang, K.L. Wang, G. X. Li, M. Saliba, D. Di Girolamo, A. Abate, Z.K. Wang, *Adv. Mater.* 32 (2020), e2003422.
- [14] Y. Lei, Y. Chen, R. Zhang, Y. Li, Q. Yan, S. Lee, Y. Yu, H. Tsai, W. Choi, K. Wang, Y. Luo, Y. Gu, X. Zheng, C. Wang, C. Wang, H. Hu, Y. Li, B. Qi, M. Lin, Z. Zhang, S. A. Dayeh, M. Pharr, D.P. Fenning, Y.H. Lo, J. Luo, K. Yang, J. Yoo, W. Nie, S. Xu, *Nature* 583 (2020) 790.
- [15] M.M. Tavakoli, K.-H. Tsui, Q. Zhang, J. He, Y. Yao, D. Li, Z. Fan, *ACS Nano* 9 (2015) 10287–10289.
- [16] Y. Wang, M. Li, X. Zhou, P. Li, X. Hu, Y. Song, *Nano Energy* 51 (2018) 556.
- [17] C. Wang, L. Guan, D. Zhao, Y. Yu, C.R. Grice, Z. Song, R.A. Avni, J. Chen, J. Wang, X. Zhao, Y. Yan, *ACS Energy Lett.* 2 (2017) 2118–2124.
- [18] B. Abdollahi Nejand, P. Nazari, S. Gharibzadeh, V. Ahmadi, A. Moshaii, *Chem. Commun. Camb.* 53 (2017) 747–750.
- [19] Z. Huang, X. Hu, C. Liu, L. Tan, Y. Chen, *Adv. Fun. Mater.* 27 (2017), 1703061.
- [20] Y. Zhao, J. Wei, H. Li, Y. Yan, W. Zhou, D. Yu, Q. Zhao, *Nat. Commun.* 7 (2016) 10228.
- [21] W. Nie, J.C. Blancon, A.J. Neukirch, K. Appavoo, H. Tsai, M. Chhowalla, M. A. Alam, M.Y. Sfeir, C. Katan, J. Even, S. Tretiak, J.J. Crochet, G. Gupta, A. D. Mohite, *Nat. Commun.* 7 (2016) 11574.
- [22] D.R. Ceratti, Y. Rakita, L. Cremonesi, R. Tenne, V. Kalchenko, M. Elbaum, D. Oron, M.A.C. Potenza, G. Hodes, D. Cahen, *Adv. Mater.* 30 (2018), 1706273.
- [23] K. Chu, B.G. Song, H.-I. Yang, D.-M. Kim, C.S. Lee, M. Park, C.-M. Chung, *Adv. Fun. Mater.* 28 (2018), 1800110.
- [24] Y. Lai, X. Kuang, P. Zhu, M. Huang, X. Dong, D. Wang, *Adv. Mater.* 30 (2018), 1802556.
- [25] Y. Lai, X. Kuang, W.-H. Yang, Y. Wang, P. Zhu, J.-P. Li, X. Dong, D.-J. Wang, Chin. J. Polym. Sci. 39 (2020) 154–163.
- [26] Z. Wu, S.R. Raga, E.J. Juarez-Perez, X. Yao, Y. Jiang, L.K. Ono, Z. Ning, H. Tian, Y. Qi, *Adv. Mater.* 30 (2018), 1703670.
- [27] C. Zuo, L. Ding, *Angew. Chem. Int. Ed.* 60 (2021) 11242.
- [28] L. Lee, J. Baek, K.S. Park, Y.E. Lee, N.K. Shrestha, M.M. Sung, *Nat. Commun.* 8 (2017) 15882.
- [29] J. Peng, J.I. Khan, W. Liu, E. Ugur, T. Duong, Y. Wu, H. Shen, K. Wang, H. Dang, E. Aydin, X. Yang, Y. Wan, K.J. Weber, K.R. Catchpole, F. Laquai, S. Wolf, T. P. White, *Adv. Energy Mater.* 8 (2018), 1801208.
- [30] Z. Zhang, Y. Gao, Z. Li, L. Qiao, Q. Xiong, L. Deng, Z. Zhang, R. Long, Q. Zhou, Y. Du, Z. Lan, Y. Zhao, C. Li, K. Müllen, P. Gao, *Adv. Mater.* 33 (2021), e2008405.
- [31] Y. Wang, Z. Zhang, Y. Lan, Q. Song, M. Li, Y. Song, *Angew. Chem. Int. Ed.* 60 (2021) 8673.
- [32] F. Liu, X. Zuo, K. Wang, H. Bao, L. Liu, Z. Guo, S. Wang, S.F. Liu, *Sol. Rrl.* 5 (2021), 2000732.
- [33] W. Xu, Y. Gao, W. Ming, F. He, J. Li, X.H. Zhu, F. Kang, J. Li, G. Wei, *Adv. Mater.* 32 (2020), e2003965.
- [34] B. Yuan, C. Li, W. Yi, F. Juan, H. Yu, F. Xu, C. Li, B. Cao, *J. Phys. Chem. Solids* 153 (2021), 110000.
- [35] T. Jiang, Z. Chen, X. Chen, X. Chen, X. Xu, T. Liu, L. Bai, D. Yang, D. Di, W.E.I. Sha, H. Zhu, Y.M. Yang, *ACS Energy Lett.* 4 (2019) 1784.
- [36] Q. He, M. Worku, L. Xu, C. Zhou, S. Lteif, J.B. Schlenoff, B. Ma, *J. Mater. Chem. A.* 8 (2020) 2039–2046.
- [37] F. Sadegh, S. Akin, M. Moghadam, V. Mirkhani, M.A. Ruiz-Preciado, Z. Wang, M. M. Tavakoli, M. Graetzl, A. Hagfeldt, W. Tress, *Nano Energy* 75 (2020), 105038.
- [38] J.-W. Lee, S.-G. Kim, S.-H. Bae, D.-K. Lee, O. Lin, Y. Yang, N.-G. Park, *Nano Lett.* 17 (2017) 4270–4276.
- [39] W. Fan, S. Zhang, C. Xu, H. Si, Z. Xiong, Y. Zhao, K. Ma, Z. Zhang, Q. Liao, Z. Kang, Y. Zhang, *Adv. Fun. Mater.* 31 (2021), 2104633.
- [40] L. Zhu, X. Zhang, M. Li, X. Shang, K. Lei, B. Zhang, C. Chen, S. Zheng, H. Song, J. Chen, *Adv. Energy Mater.* 11 (2021), 2100529.
- [41] Y. Rao, Z. Li, D. Liu, C. Chen, X. Wang, G. Cui, S. Pang, *ACS Appl. Mater. Interfaces* 13 (2021) 20043.
- [42] Z. Liu, S. Li, X. Wang, Y. Cui, Y. Qin, S. Leng, Y.-X. Xu, K. Yao, H. Huang, *Nano Energy* 62 (2019) 734–744.
- [43] Y.-D. Wang, Y. Wang, J.-Y. Shao, Y. Lan, Z.-R. Lan, Y.-W. Zhong, Y. Song, *ACS Energy Lett.* 6 (2021) 2030–2037.
- [44] F.F. Targhi, Y.S. Jalili, F. Kanjouri, *Results Phys.* 10 (2018) 616–627.
- [45] Y. Wang, X. Zhou, C. Liang, P. Li, X. Hu, Q. Cai, Y. Zhang, F. Li, M. Li, Y. Song, *Adv. Electron. Mater.* 3 (2017), 1700169.
- [46] B.P. Finkenauer, Y. Gao, X. Wang, Y. Tian, Z. Wei, C. Zhu, D.J. Rokke, L. Jin, L. Meng, Y. Yang, L. Huang, K. Zhao, L. Dou, *Cell Rep. Phys. Sci.* 2 (2021), 100320.
- [47] Q. Zhang, J. Duan, Q. Guo, J. Zhang, D. Zheng, F. Yi, X. Yang, Y. Duan, Q. Tang, *Angew. Chem. Int. Ed.* 61 (2022), e202116632.



Yangjie Lan received his master's degree in 2021 from Institute of Chemistry, Chinese Academy of Sciences, under the supervision of Prof. Yanlin Song. Now he is a Ph.D. candidate at the School of Chemistry and Chemical Engineering, Beijing Institute of Technology. His research interests focus on perovskite solar cells.



Yang Wang received his Ph. D. degree in material physics and chemistry from Beihang University in 2016. Now he is an associate professor at the Key Laboratory of Green Printing, ICCAS. His research interests include organic-inorganic hybrid optoelectronics such as solar cells, printing photoelectric devices.



Yue Lai received her Ph.D. degree from the Institute of Chemistry, Chinese Academic of Sciences in 2020. Her research focuses on the structure and properties of stimuli-responsive polyurethane controlled by dynamic covalent bonds.



Mingzhu Li is a professor of the Institute of Chemistry, Chinese Academy of Sciences (ICCAS). Her research interest focuses on the design of highly effective optical antennas using photonic crystals and other bioinspired optical structures.



Mingquan Tao received his Bachelor's degree from University of Chinese Academy of Sciences in 2020. He is a Ph. D. candidate under the supervision of Prof. Yanlin Song in Institute of Chemistry, Chinese Academy of Sciences (ICCAS). Now his research focuses on inverted perovskite solar cells.



Xia Dong is an in-service doctoral supervisor at the Institute of Chemistry, Chinese Academy of Sciences. Her research focuses on the molecule design and preparation of new thermoplastic elastomers and microstructure control and performance enhancement of polymeric materials.



Zheren Cai received his PhD in Institute of Chemistry, Chinese Academy of Sciences (ICCAS) in 2021. Now he is a postdoctoral researcher in School of Materials Science and Engineering, Nanyang Technological University (NTU). He Now his research focuses on wearable devices



Yanlin Song received his Ph. D. degree from the Department of Chemistry at Peking University in 1996. Then he conducted research as a postdoctoral fellow at Tsinghua University from 1996 to 1998. He has been working at ICCAS since 1998. His research interests include nano-materials and green-printing technology, printed electronics and photonics, fabrication and applications of photonic crystals. He has published more than 400 papers, 14 books and chapters, and has been granted more than 130 patents from China, USA, European Union, Japan and Korea, etc.



Yuduan Wang received his master's degree in 2021 from Institute of Chemistry, Chinese Academy of Sciences, under the supervision of Prof. Yuwu Zhong. He is currently a PhD candidate at the Department of Chemical and Biomolecular Engineering in National University of Singapore. His research interests focus on perovskite solar cells.